Biosensors and Bioelectronics 230 (2023) 115234

Contents lists available at ScienceDirect

Biosensors and Bioelectronics

journal homepage: www.elsevier.com/locate/bios

Modified glucose as a sensor to track the metabolism of individual living endothelial cells - Observation of the 1602 cm^{-1} band called "Raman spectroscopic signature of life"

Anna Pieczara [a,b], Aleksandra Borek-Dorosz [c], Szymon Buda [c], William Tipping [d], Duncan Graham [d], Robert Pawlowski [e], Jacek Mlynarski [e], Malgorzata Baranska [a,c,*]

[a] Jagiellonian Centre for Experimental Therapeutics (JCET), Jagiellonian University, 14 Bobrzynskiego Str., 30-348, Krakow, Poland
[b] Jagiellonian University in Kraków, Doctoral School of Exact and Natural Sciences, 11 Lojasiewicza St., Krakow, Poland
[c] Faculty of Chemistry, Jagiellonian University, 2 Gronostajowa Str., 30-387, Krakow, Poland
[d] Centre for Molecular Nanometrology, WestCHEM, Department of Pure and Applied Chemistry, Technology and Innovation Centre, University of Strathclyde, Glasgow, G1 1RD, United Kingdom
[e] Institute of Organic Chemistry, Polish Academy of Sciences, 44/52 Kasprzaka Str., 01-224, Warsaw, Poland

ARTICLE INFO

Keywords:
3-OPG glucose
Endothelium
Spontaneous Raman microscopy
Stimulated Raman scattering

ABSTRACT

A relatively new approach to subcellular research is Raman microscopy with the application of sensors called Raman probes. This paper describes the use of the sensitive and specific Raman probe, 3-*O*-propargyl-D-glucose (3-OPG), to track metabolic changes in endothelial cells (ECs). ECs play a significant role in a healthy and dysfunctional state, the latter is correlated with a range of lifestyle diseases, particularly with cardiovascular disorders. The metabolism and glucose uptake may reflect the physiopathological conditions and cell activity correlated with energy utilization. To study metabolic changes at the subcellular level the glucose analogue, 3-OPG was used, which shows a characteristic and intense Raman band at 2124 cm^{-1}.3-OPG was applied as a sensor to track both, its accumulation in live and fixed ECs and then metabolism in normal and inflamed ECs, by employing two spectroscopic techniques, i.e. spontaneous and stimulated Raman scattering microscopies. The results indicate that 3-OPG is a sensitive sensor to follow glucose metabolism, manifested by the Raman band of 1602 cm^{-1}. The 1602 cm^{-1} band has been called the *"Raman spectroscopic signature of life"* in the cell literature, and here we demonstrate that it is attributed to glucose metabolites. Additionally, we have shown that glucose metabolism and its uptake are slowed down in the cellular inflammation. We showed that Raman spectroscopy can be classified as metabolomics, and its uniqueness lies in the fact that it allows the analysis of the processes of a single living cell. Gaining further knowledge on metabolic changes in the endothelium, especially in pathological conditions, may help in identifying markers of cellular dysfunction, and more broadly in cell phenotyping, better understanding of the mechanism of disease development and searching for new treatments.

1. Introduction

Raman microscopy (RM) is one of the most powerful tools for studying the molecular structure of biological samples *in vitro*, *ex vivo,* and *in vivo*. RM relies on inelastic scattering of the incident light by molecules, allowing the molecular composition of cells and tissues to be investigated in a label-free manner (Raman and Krishnan, 1928; Hamada et al., 2008; Małek, 2016). This technique has many advantages, i.e. it provides information simultaneously about several components, it is relatively specific and selective, it is non-destructive, and it requires only minimal sample preparation (Baranska et al., 2015; Sato et al., 2019). Due to the numerous advantages, optical methods are attractive tools in cell biology, medicine, and pharmaceutical science. However, given the targeted research activities in intricate biological systems, optical labels proved to be very useful. The most common fluorescence dyes are only suitable for restrictive analysis and they are comparatively much larger in terms of molecular weight in comparison to the conjugated biomolecules, which can significantly change biological activity. (Li et al., 2017; Yamakoshi et al., 2012). A relatively new approach to subcellular research is Raman imaging with the

* Corresponding author. Jagiellonian Centre for Experimental Therapeutics (JCET), Jagiellonian University, 14 Bobrzynskiego Str., 30-348, Krakow, Poland.
E-mail address: m.baranska@uj.edu.pl (M. Baranska).

https://doi.org/10.1016/j.bios.2023.115234
Received 11 December 2022; Received in revised form 6 March 2023; Accepted 13 March 2023
Available online 15 March 2023

application of Raman probes (Rp). Compared to the label-free approach, which is limited to species that occur in substantial amounts in cells, such as lipids and proteins, the labeled approach can improve selectivity and sensitivity for the observation of organelles in cells and, more significantly, allows the tracing of cellular changes. These specific chemical structures, which are delivered to the cells in very low concentrations, target specific organelles and enable their imaging, in a faster and more effective manner than the label-free approach. Rp consists of the targeting moiety and a Raman-active group, such as alkyne (C≡C), nitrile (C≡N), and deuterium (C-D), that show a distinct, strong Raman band in a cellular-silent region for biological samples (1800–2800 cm^{-1}). As a result, the spectra obtained from a particular cellular area show exactly where the Rp accumulates, allowing a more sensitive and selective localization of individual organelles (Li et al., 2017; Matuszyk et al., 2021; Yamakoshi et al., 2012). Although powerful, RM suffers from the speed of image acquisition when looking at single or preferably multiple cells and can be prone to autofluorescence interference. An advanced form of RM is stimulated Raman scattering (SRS) microscopy which overcomes some of the limitations of RM. In addition, SRS provides excellent measurement confocality and is autofluorescence background free (Hamaguchi and Iwata, 2017).

SRS microscopy is a nonlinear optical method that enables fast imaging due to signal enhancement of up to 10^8 times. Two ultrafast pulsed laser lines referred to as the pump and Stokes beams, are necessary to acquire SRS images. As SRS is much faster than RM, this approach has gained popularity and is being used more and more (Brzozowski et al., 2022; Liao and Cheng, 2016). In the beginning, the main interest of SRS microscopy applications was label-free imaging. Label-free SRS has been used to detect molecular species with intrinsic chemical bonds in the high-frequency region (2800−3050 cm^{-1}) (Freudiger et al., 2008; Ji et al., 2013; Wang et al., 2013) and cellular fingerprint region (500−1800 cm^{-1}) (Wang et al., 2013; Zhang et al., 2012). In addition, the labeled approach has been rapidly developed in the past decade (Wei et al., 2014; Palonpon et al., 2013; Miao et al., 2021). Exogenous tags may contribute to providing additional temporal information related to the metabolic turnover of labeled species within cells, which are often missing from label-free imaging. A new field of bio-orthogonal chemical imaging has been developed as a result of SRS microscopy coupled with Rp, which allows dynamic visualization of many small molecules in living systems (Brzozowski et al., 2022; Wei et al., 2016).

The use of sensors is very wide in different fields of science, from biological applications (Wei et al., 2014, 2017; Yamakoshi et al., 2012) to material science (Ao et al., 2020; Fleury and Roeffaers, 2020; Laptenok et al., 2020). Besides the biological applications, one of the interesting fields are studies regarding sensors ensemble materials used, among others in the detection of ions (Awual, 2017, 2019a) or capturing of hazardous dyes and ions from water (Awual, 2019b; Hasan et al., 2021; Kubra et al., 2021), which also are important for human health. In the presented manuscript the topic focused on a very narrow specific field, the sensors which are biologically active and can be easily tracked with the use of Raman spectroscopy techniques.

Endothelial cells (ECs) are very often erroneously perceived as an inert single layer that lines the circulatory system, which only guides and conducts blood, whereas they play a significant role in a healthy and dysfunctional state (Eelen et al., 2015; Rajendran et al., 2013). Dysfunction of endothelium is one of the important factors in the occurrence of cardiovascular diseases and some types of cancer (Galley and Webster, 2004; Potente and Carmeliet, 2017; Rajendran et al., 2013). As understanding of ECs metabolism has increased over the past few years, cellular metabolic pathways are positioned as central mediators of signaling in health and disease. The energy needs of ECs are highly dependent on glucose as it serves as the primary metabolic fuel. ECs have a relatively low mitochondria content (6–18%) and rely mainly on glycolysis rather than oxidative phosphorylation (Eelen et al., 2015; Wong et al., 2017). Glycolysis is defined as a chain of reactions in which one molecule of glucose is broken down into two molecules of pyruvate, leading to the production of ATP in mitochondria (Yetkin-Arik et al., 2019). In the first stage of glycolysis, glucose is converted to glucose-6-phosphate (G6P), which is also a substrate in the uronic acid cycle (glycocalyx and protein glycosylation) and the pentose phosphate pathway (amino acids synthesis). G6P is converted to fructose-6-phosphate (F6P), which is involved in the hexamine pathway (glycocalyx and protein glycosylation). F6P is transformed then into fructose-1,6-bisphosphate (F1,6P2), glyceraldehyde-3-phosphate (G3P), and 3-phosphoglycerate (3 PG), which is directly converted into the main glycolysis product pyruvate. The pyruvate formed during glycolysis enters mitochondria and then is converted to acetyl-coenzyme and engages in the tricarboxylic acid cycle (TCA), the major energy-generating metabolic pathway in cells (Pircher et al., 2016). There are many advantages to using glycolysis in ECs as the main energy source, such as; lower level of reactive oxygen species (ROS) produced during oxidative phosphorylation and prevention of apoptotic cell death in an oxidative stress environment (Yetkin-Arik et al., 2019), ATP production with faster kinetics (Du et al., 2021) and providing metabolic intermediates for the generation of amino acids, lipids, proteins, and nucleotides (Zhu and Thompson, 2019). In the dysfunctional state of cells, glucose metabolism, and more precisely glucose uptake, becomes weakly controlled. To follow changes in glucose metabolism, it is important to understand cell activity correlated with energy metabolism, under both normal and pathological conditions (Hu et al., 2015). Gaining further knowledge about metabolic patterns in the endothelium, and especially in the various pathologies affecting ECs, should open valuable opportunities for entirely novel treatment approaches (Pober and Sessa, 2007; Pircher et al., 2016).

Glucose analogues labeled with fluorescent dyes have been developed to investigate glucose metabolism by imaging techniques at a single-cell resolution. However, fluorescent glucose analogues display perturbed behaviors and unwanted interactions in cells due to their relatively big size, thereby biasing glucose metabolism. To overcome this problem, a new approach based on the Rp is being developed. Specifically, glucose was labeled with deuterium or a small alkyne tag at the 3-position, which allows a signal to be obtained in the silent region of the Raman spectrum. Previous studies have shown that those analogues have very little non-specific interaction, unlike the fluorescence probe versions (Hu et al., 2015; Long et al., 2017). Glucose-based Rps have found their application in research related to the uptake and tracking of glucose metabolism in cells and tissues (Hu et al., 2015). In tumour tissues and neuronal culture, 3-*O*-propargyl-D-glucose (3-OPG) was utilized to discriminate cancer cells with distinct metabolic activity and reveal heterogeneous glucose uptake patterns at the cellular level (Hu et al., 2015). The ability to detect different Raman spectral fingerprints for C-D bonds in the macromolecules produced, and use them for macromolecule-type-specific metabolic mapping with high spatial resolution, was made achievable by using deuterium-labeled glucose (Zhang et al., 2019). The new 3-OPG-$^{13}C_3$ probe, which uses a ^{13}C-isotope editing technique, made it possible to examine the glucose uptake and incorporation activity in cells and mice brain tissues (Long et al., 2017). The glycolysis process, in which alkyne glucose takes part, due to the presence of an alkyl group in the third position, stops at the stage of converting fructose 1,6-bisphosphate to glyceraldehyde 3-phosphate and dihydroxyacetone phosphate. The stoppage of the pathway at this stage is due to the inability to attach the phosphate group that would attach in the third position (Hu et al., 2015).

Observation of metabolic changes in the cell by a label-free approach is possible due to the very rare (mostly observed in yeast cells) band at 1602 cm^{-1} (Huang et al., 2007, 2004). The 1602 cm^{-1} Raman signature, which was named the *Raman spectroscopic signature of life*, is a Raman marker band for cell (mitochondria) metabolic activity. Although its intensity sensitively reflects the metabolic status of the cell, its molecular origin remained unclear (Chiu et al., 2012). The studies postulated that this unidentified band is most likely derived from a molecule present in the mitochondria. They concluded by considering that

mitochondria are organelles whose membranes are rich in phospholipids and the fact that this band was present in spectra with bands characteristic of phospholipids (confirmed by comparing to the spectrum of phosphatidylcholine) (Huang et al., 2003). It has also been shown that this band may originate in yeast cells from ergosterol, which is part of the cell membrane (Chiu et al., 2012) and can be closely related to haem functions in the cell (Chiu and Hamaguchi, 2011).To verify if the *Raman spectroscopic signature of life* is limited to particular cells, Pully and Otto (2009) showed its presence in eukaryotic cells of four different origins (HeLa cells, peripheral blood lymphocytes, human mesenchymal stem cells, and bovine chondrocytes). They noticed that the intensity of the 1602 cm^{-1} band varied with cell type (most intense for HeLa cells), but it may be due to different concentrations of mitochondria in the cells.

As highlighted above, tracking changes in cell metabolism is important in identifying markers of cellular dysfunction. The study of genomics reveals what a cell is capable of, while transcriptomics shows what it is planning to do. As such, proteomics and metabolomics are necessary for finding out what cells do. An analysis of metabolites provides the best insight into a cell's chemical processes (Seydel, 2021). Localization of metabolic changes in a single cell is quite challenging. There are several standard protocols for analyzing the structure and function of cells, including immunophenotyping (flow cytometry) (Bleesing and Fleisher, 2001), molecular techniques (RNA/DNA sequencing) (Wang et al., 2020), and histochemical examination (Ji and Kato, 2001). Mass spectrometry is currently the method of choice for metabolomic analysis of bulk samples (Theodoridis et al., 2011). However, these protocols do not provide information about cell metabolomic status. It is worth emphasizing that RM and SRS microscopy can be used to study complex metabolic profiles in live cells and tissue under both physiological and pathological conditions with single-cell resolution and minimal perturbation (Hu et al., 2016; Jamieson et al., 2018a; Lalonde et al., 2021).

In this paper, we investigate the uptake and metabolism of glucose both by normal and inflamed ECs. The alkyne-labeled glucose, 3-OPG, was used as a sensitive Rp to track its accumulation and then metabolism in human aorta endothelial cells (HAEC). Inflammation of the cells was modeled by TNF-α. Measurements were conducted using RM, which allows full spectral information to be gathered from cells, and SRS imaging to increase the speed of measurement, and hence, the number of measured cells. To the best of our knowledge, this is the first report of glucose metabolism in EC obtained from single living cells, which also verifies if the origin of the *Raman spectroscopic signature of life* is really showing mitochondrial activity.

2. Materials and methods

2.1. Synthesis of Raman probe

To a solution of S1 (1 g, 3.84 mmol) in DMF (10 mL) was added sodium hydride (0.185 g, 7.68 mmol) at 0 °C and stirred for 10 min. Then, propargyl bromide (0.346 mL, 4 mmol) was added and stirred at room temperature for 16 h. After completion (TLC), the reaction mixture was diluted with water (20 mL) and extracted in ethyl acetate (3 × 20 mL). Pooled organic layers were washed with brine (20 mL), dried over $MgSO_4$, and the solvent was removed under reduced pressure and crude was purified by silica gel column chromatography (Hexane: EA 3:1) to furnish S2 as a yellowish oil (1.15 g, 99%).

To a suspension of S2 (1.15 g, 3.83 mmol) in water (20 mL) was added DOWEX 50WX8 H^+ (0.3 g). Then the reaction mixture was stirred at 80 °C for 2h. After completion (TLC), the resin was removed by filtration and the reaction mixture was concentrated under reduced pressure. The crude product was purified by crystallization (DCM/MeOH) to furnish 3-OPG as a colorless powder as a mixture of α/β-anomers. (0.72 g, 86%). NMR data of 3-OPG (Fig. S1) is consistent with the literature (Hu et al., 2015).

2.2. Cell culture

HAECs (Gibco, Lonza) were cultured in the supplemented endothelial cell growth EGM-2MV medium from Lonza and grown at 37 °C in constantly humidified air conditions with 5% CO_2 content. For RM measurement HAEC were seeded directly onto CaF_2 windows, in the amount of approximately 150 000 per slide, for SRS measurement HAEC were seeded directly onto a glass bottom Petri dish (35 mm Glass bottom dish with 20 mm micro-well, Cellvis), in the amount of approximately 70 000 per dish, after time enough for cells to proliferate and spread, enabling them to reach optimal confluence (approximately 24h). Prior to Raman measurement, cells were treated with 3-OPG (25 mM, 24h), TNF-α (10 ng/mL, 3h), and mannitol (20 mM, 24h) (Sigma-Aldrich). For measurement of the fixed cells, they were next exposed to 2.5% glutaraldehyde solution for 5 min, then rinsed three times in PBS (pH ~7.4) and stored at 4 °C until the execution of the measurement.

2.3. Raman imaging

Raman imaging was accomplished using WITec Confocal Raman Microscope (WITec GmbH, Ulm, Germany), supplied with an Ultra-High-Throughput Screening (UHTS) 300 spectrograph and a charge-coupled device (CCD) detector (Andor, DU401A-BV- 352) operated *via* WITec Control Software. All spectra were collected with a laser excitation of 532 nm, a black-illuminated CCD camera, and a 40 × water immersion objective (Nikon Fluor; NA = 1). All spectra were collected in the range 3670–0 cm^{-1}, with a spectral resolution of 3 cm^{-1}. The spatial resolution possible with this setup is approximately 0.36 μm. The size of the mapped area was dependent on cell size and was adjusted individually. The sampling density for measured cells was 0.5–0.6 μm depending on cell size and the integration time of 0.1 s. Analysis of Raman imaging data enables the creation of Raman images based on the integral intensity of selected bands, showing the distribution of cellular components, i.e. organic matter (3015–2815 cm^{-1}), lipids (2860–2840 cm^{-1}), alkyne group of 3-OPG (2124 cm^{-1}), Raman signature of life (1602 cm^{-1}) and cytochrome *c* (755 cm^{-1}). From each sample, up to 10 cells were imaged.

2.4. SRS imaging

An integrated laser system (picoEMERALD™ S, Applied Physics & Electronics, Inc. Berlin) was used to produce two synchronized laser beams at an 80 MHz repetition rate. A fundamental Stokes beam (1031.4 nm, 2 ps pulse width) was intensity modulated by an electro-optic-modulator with >90% modulation depth, and a tunable pump beam (700–960 nm, 2 ps pulse width, <1 nm (~10 cm^{-1}) spectral bandwidth) was produced by a built-in optical parametric oscillator. The pump and Stokes beams were spatially and temporally overlapped using two dichroic mirrors and a delay stage inside the laser system and coupled into an inverted laser-scanning microscope (Leica TCS SP8, Leica Microsystems) with optimized near-IR throughput. SRS images were acquired using a 40 × objective (HC PL IRAPO 40 × , N.A. 1.10 water immersion lens) with a 48.82 μs pixel dwell time over a 145.31 × 145.31 μm frame. The Stokes beam was modulated with a 20 MHz EoM (Zurich Instruments). Forward scattered light was collected by an S1 N. A. 1.4 condenser lens (Leica Microsystems). Images were acquired at 12-bit image depth. The power of the Stokes beam was 0.3W and the pump 0.15 W. Label-free SRS imaging within the high wavenumber region of the Raman spectrum (2800-3050 cm^{-1}) with the spatial resolution of the system is ~400 nm (pump wavelength = 792 nm). The images were collected at pump beams: 789.6 nm (2970 cm^{-1}), 792.0 nm (2930 cm^{-1}), 797.2 nm (2850 cm^{-1}), 846.1 nm (2124 cm^{-1}) and 885.1 nm (1602 cm^{-1}). Additionally, SRS spectra were collected in the ranges of: 2810 - 3050 cm^{-1} (799.6–784.5 nm), 2060 - 2200 cm^{-1} (850.6–839.2 nm) and 1416 - 1703 cm^{-1} (899.9–877.3 nm) with a 50 Hz acquisition rate. From each sample, up to 30 cells were imaged.

2.5. Data analysis and processing

Raman data were analyzed using WITec Plus software (WITec GmbH). Preprocessing of Raman spectra included Cosmic Ray Removal (CRR; filter size: 4; dynamic factor: 4) and Background Subtraction (BG; polynomial order: 3). The spectra prepared this way were analyzed by *k*-means cluster analysis (KMCA) in the range of 3050–2800 cm^{-1} and 1800–500 cm^{-1}. As a result of cluster analysis, average spectra were obtained for various cell components (i.e. cytoplasm, cell nucleus, lipids, and additionally cytoplasm region with a high content of cytochrome *c* in the case of living cells). Average Raman spectra were obtained by averaging spectra from individual classes from KMC analysis (i.e., cytoplasm, nucleic acids, lipids, and cytochrome *c*) for 5–6 cells. The Raman spectra presented here are shown in the range of 3050–500 cm^{-1} and were normalized using the Opus software (Bruker). For data presentation Origin 2021 (OriginLab Corporation) and GraphPad Prism 9 (GraphPad Software) were used.

The analysis of the SRS images was performed in ImageJ software. Ratiometric images were generated based on raw frames collected for lipids (2851 cm^{-1}), alkyne group (2124 cm^{-1}), and glucose metabolite (1602 cm^{-1}). The frames collected for protein (2930 cm^{-1}) were used to normalize acquired frames (the fluctuation of intensity) following the approach described by Bik (Bik et al., 2022) and Jamieson (Jamieson et al., 2018b). In the next step, the ratios 2850 cm^{-1}/(2930 cm^{-1}+2850 cm^{-1}), 1602 cm^{-1}/(2930 cm^{-1}+1602 cm^{-1}), and 2124 cm^{-1}/(2930 cm^{-1} +2124 cm^{-1}) were calculated with the Image Calculator option in Image J, then for each cell on the images, the values were acquired with the function Measure. The values were further visualized in box and whisker form in Origin software.

3. Results and discussion

3.1. Characterisation of 3-OPG

The modified glucose was first investigated by spontaneous RM (Fig. 1). This allowed us to gain insight into its structure and a unique spectral signature with a characteristic band in the silent region. For the identification of modified glucose, a very intense alkyne band positioned at 2124 cm^{-1} can be used. The occurrence of this band in the silent region of the Raman spectrum of cells incubated with this Rp, in which most endogenous molecules do not exhibit Raman scattering, is a good sensor to track cell metabolism. In normal conditions, cells do not possess any bands in this range. Tracking cellular changes related to this molecule (i.e. using this band) will involve unambiguously attributing it to changes in the glucose pathway.

The literature in the field of click-chemistry, which also used alkyne tag (Grammel and Hang, 2013; Prescher and Bertozzi, 2005), of which the 3-OPG sensor is composed, this bond is chemically inert and biorthogonal (without interfering with native biochemical processes). Compared with fluorophores used in fluorescence imaging which are relatively bulky and often considerably alter biological activity, the alkyne tag is much smaller and do not interfere with the functioning of the cell. Also, the use of 3-OPG sensor does not require the use of radioactive isotopes, which could be more harmful to the cells (Hu et al., 2015; Li et al., 2017).

3.2. Distribution of 3-OPG in normal HAEC

Modified glucose was detected at first in live ECs, which were incubated with 25 mM 3-OPG at different times. To reveal the biological activity of 3-OPG, it was important to obtain detailed information about its intracellular distribution and how it evolves with time. Fig. 2 shows representative Raman images of live HAEC incubated with a 3-OPG for 1h, 6h, 12h, 18h, and 24h, respectively. Raman images were obtained by the integration of characteristic bands of selected cell components, i.e. organic matter (2815–3015 cm^{-1}), lipids (2840–2860 cm^{-1}), cytochrome *c* (745 - 765 cm^{-1}), 1597 - 1607 cm^{-1} (glucose metabolite) and 2114 - 2134 cm^{-1} (3-OPG). These images indicated the localization of specific cellular organelles, e.g. ER-rich area (lipids), mitochondria (cytochrome *c*), lipid droplets (aggregated lipids), or cytoplasm (protein-rich class).

The obtained data show that the intensity of the 2124 cm^{-1} band is very low in the analyzed cells, even after a long incubation e.g. 18, 24h. After 12 h, a slight increase in the intensity of the signal can be observed, which enables the estimation of the distribution of the alkyne group inside the cells. The low intensity of the signal causes difficulties in the determination of the exact localization of modified glucose inside the cell, let alone co-localization with other subcellular structures. It seems that it accumulates strongly in the perinuclear region which may correlate to the ER. It is worth emphasizing that the glycolysis process, in which alkyne glucose takes part due to the presence of an alkyl group in the third position (Fig. 1), is stopped at the stage of converting fructose 1,6-bisphosphate to glyceraldehyde 3-phosphate and dihydroxyacetone phosphate. The stoppage of the pathway at this stage is due to the inability to attach the phosphate group that would attach in the third position. Virtually all cellular components, i.e. proteins, lipids and nucleotides, are formed from the glycolysis products until the glycolysis is stopped, which involves an alkylated analogue of glucose.

3.3. Observation of 1602 cm^{-1} band, called the Raman spectroscopic signature of life

By carefully analyzing the cells that were treated with modified glucose, it was possible to see a change in the 1602 cm^{-1} band, which is not present at all in the control cells, while an increase in its intensity can be seen with incubation time. In addition, it was verified that

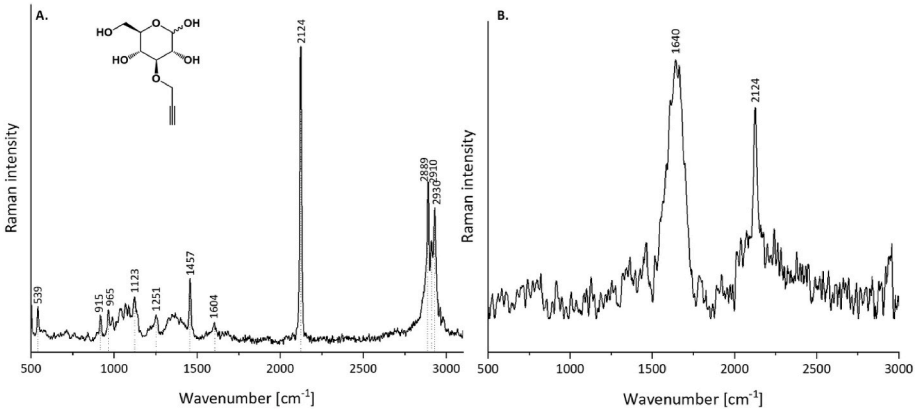

Fig. 1. Chemical structure and Raman spectrum of 3-O-propargyl-D-glucose (3-OPG): A. solid and B. dissolved in water (10 mM).

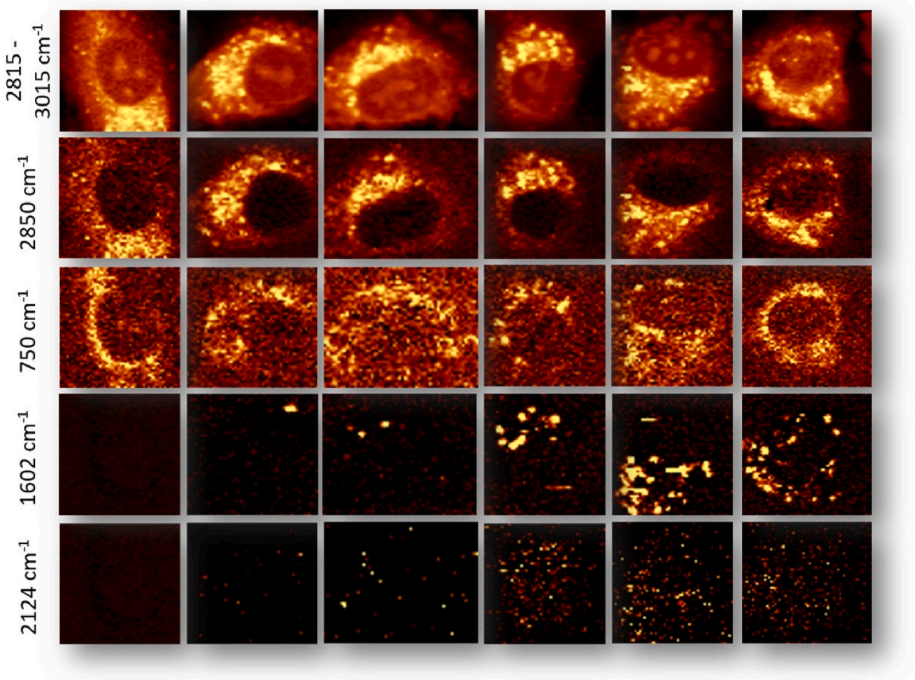

Fig. 2. Raman images of live HAEC cells incubated with 3-OPG (25 mM) by 0, 1, 6, 12, 18 and 24h, obtained by the integration of Raman bands in the regions: 2815 - 3015 cm^{-1} (organic matter), 2840 - 2860 cm^{-1} (lipids), 745 - 765 cm^{-1} (cytochrome *c*), 1597 - 1607 cm^{-1} (glucose metabolite) and 2114 - 2134 cm^{-1} (3-OPG).

incubation with glucose did not cause a similar effect. It has been shown that incubation of cells with glucose does not cause the appearance of the 1602 cm^{-1} band in their Raman spectrum (data shown in supplementary information). In contrast, when using 3-OPG, the presence of this band can be visible after 1h, but its localization in cells can be estimated with no doubt after 12h. Based on that, it can be concluded that the modified glucose was metabolized by the endothelial cells as manifested by the appearance of a band at 1602 cm^{-1}. This band called the *Raman spectroscopic signature of life* first was reported in yeasts (Chiu and Hamaguchi, 2011; Huang et al., 2004). It is a marker Raman band for cell metabolic activity. Even though its intensity sensitively reflects the metabolic status of the cell, its molecular origin remained unclear (Chiu et al., 2010; Huang et al., 2007). It was postulated that this unidentified band was most likely derived from a specific molecule occurring in mitochondria (Pully and Otto, 2009), but it was also proposed that ergosterol is the major contributor to the 1602 cm^{-1} band (Chiu et al., 2012). This band is also assigned with terminal groups NH_3^+ and COO^-, characteristic of amino acids (Wen et al., 2021; Zhu et al., 2011). It is noteworthy that the spectrum of unprocessed alkylated glucose does not have a band at 1602 cm^{-1}, which was also confirmed by the performed calculations. As was emphasized in the introduction, glucose is involved in many metabolic pathways and is the substrate of most of the compounds that build the cell. Our modification of glucose in its structure contains an additional alkyl group, which is a relatively reactive group. Due to its reactivity, the alkyl group can react in a specific way with cellular components, i.e. proteins, lipids, and also heavy metals present in proteins, and therefore a specific enzymatic reaction takes place, which results in the observation of a very intense 1602 cm^{-1} band. It can also be postulated that the high glucose state, by changing the pH even slightly, may cause changes in the resulting metabolites, which allows the observation of the 1602 cm^{-1} band. The next hypothesis is that in contrast to glucose, 3-OPG cannot be phosphorylated as that would occur with glucose, so alternative pathways are activated in an attempt to overcome this non-natural substrate. Our finding may indicate that cells incubated with modified glucose are metabolized, which is reflected by a characteristic signal. We cannot specify exactly, which metabolite is responsible for this band, however, it may be related to enzymatic oxidation of glucose.

Raman images may be ambiguous and difficult to interpret, especially when comparing the full chemical information, for this reason, the application of chemometric methods was necessary. By applying the analysis of characteristic bands and KMC analysis (Fig. 2), the spectra corresponding to the individual subcellular compartments were possible to extract. Additionally, these methods allow us to obtain maps that show the locations of alkyne glucose, which was visualized and embedded by using the integration of the 2124 cm^{-1} band. The analysis shows that the alkyne-derived (C≡C) band is present in three classes, i.e. cytochrome *c*-rich cytoplasm class, cell nucleus class, and "poor" cytoplasm, in which the presence of the bands characteristic for individual cell-like lipids or cytochrome *c* components were not identified.

In our study, the longer incubation times resulted in the increased intensity of this band and a larger area in the cell (Fig. 3). This band is better specified, the distribution is partially in line with that of the cytoplasm with high content of lipids and the cytochrome *c* classes.

3.4. Uptake and metabolism of 3-OPG by normal and inflamed HAEC

In a further step to verify whether we can track the glucose metabolism in inflamed cells, the cells were incubated with 3-OPG (5 and 25 mM), both control and inflamed (preincubated with TNF- α for 24h). The pathological state of ECs caused by TNF-α has already been studied, which shows that cells treated with TNF-α showed the increased production of lipid droplets (LDs), mainly composed of unsaturated lipids (Czamara et al., 2017; Pacia et al., 2020).

The differences in uptake of alkylated glucose by normal and TNF-α treated cells were first analyzed by application of RM. At low concentrations (5 mM, data presented in supplementary information) the signal from the ν(C≡C) group, and the 1602 cm^{-1} band, were hardly observed. The incubation with 3-OPG at a high concentration (25 mM) resulted in higher intensity of ν(C≡C), which in recorded images provides information about the subcellular localization of the probe. Fig. 4 shows representative Raman images based on integration of the spectral range of 2815–3015 cm^{-1}, displaying a region of the whole cell (organic matter), bands 2840-2860 cm^{-1} displaying a region rich in lipids, 745-

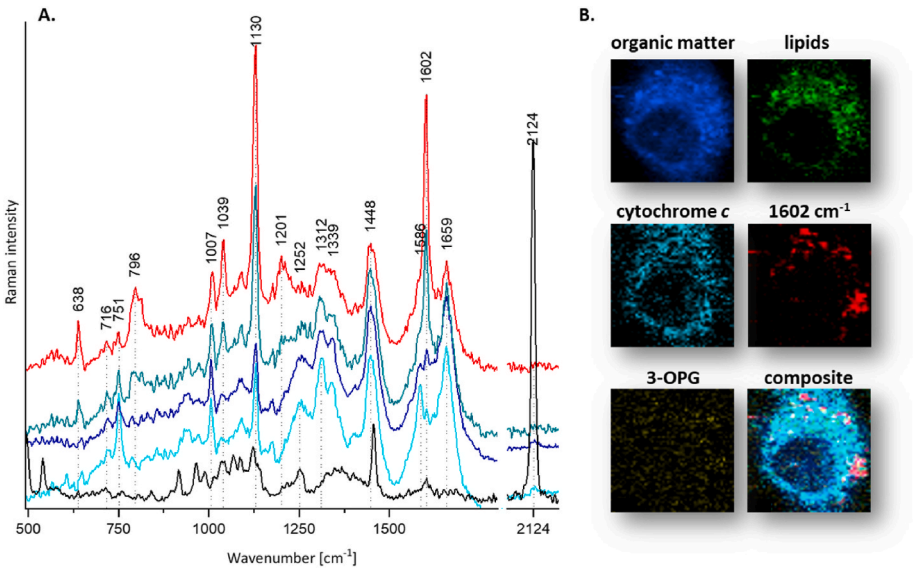

Fig. 3. KMC of representative HAEC incubated with 3-OPG (25 mM, 24h). A. The average Raman spectra of the KMC characteristic classes: cytochrome *c* (cyan, 745-765 cm^{-1}), organic matter (blue, 2815-3015 cm^{-1}), lipids (green, 2830-2900 cm^{-1}), and glucose metabolite (red, 1597 - 1607 cm^{-1}) and standard Raman spectrum of 3-OPG (black). B. Raman distribution maps of presented classes in A with their overlay (composite).

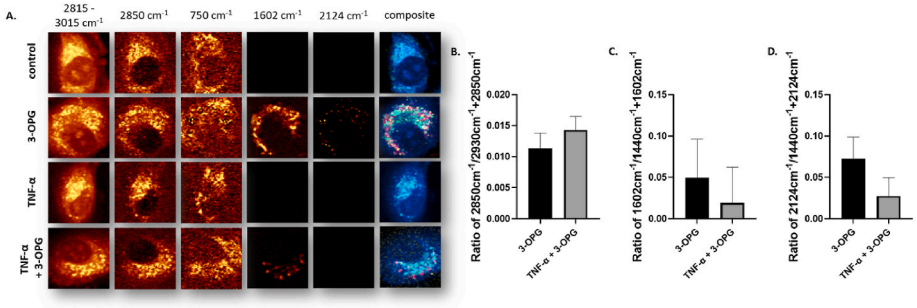

Fig. 4. Raman images of live HAEC cells upon 3-OPG (25 mM, 24h) uptake in normal and pathological conditions (TNF-α treated cells). Representative Raman images obtained by the integration of the selected Raman bands at 2815-3015 cm^{-1} (organic matter), 2840-2860 cm^{-1} (lipids), 745-765 cm^{-1} (cytochrome *c*), 1597-1607 cm^{-1} (glucose metabolite) and 2114-2134 cm^{-1} (3-OPG). False color images displaying the distribution of selected cell components (organic matter -blue), lipids - green, 1602 cm^{-1} -red, and alkyne group - yellow) and their colocalization in the composite image. Quantitative ratiometric analysis of the ratio of B. 2850 cm^{-1}/(2930 cm^{-1}+2850 cm^{-1}), C. 1602 cm^{-1}/(1440 cm^{-1}+1602 cm^{-1}) and D. 2124 cm^{-1}/(1440 cm^{-1}+2124 cm^{-1}) for RS images. Error bar: standard deviation.

765 cm^{-1} showing cytoplasm with high content of cytochrome *c*, 1602 cm^{-1} shows the glucose metabolite distribution, while 2124 cm^{-1} shows the accumulation of modified glucose.

In the cells undergoing inflammatory responses, the bands characteristic for lipids were more intense and the formation of more dense lipid clusters were observed in comparison to the control cells. While in contrast, the intensity of the signal corresponding to 1602 cm^{-1} resulting from the metabolism of external glucose was lower in cells pre-treated with TNF-α, than in normal conditions. Such a decrease and, in addition, the 2124 cm^{-1} bands may also suggest a reduced uptake, which was also noted earlier in the example of deuterated acids (Borek-Dorosz et al., 2022).

To compare quantitatively the changes in lipid accumulation in inflamed and control HAEC after 3-OPG administration, the intensity of bands at 2850 cm^{-1} and 2930 cm^{-1} were calculated, as well as a ratio of 2850 cm^{-1}/(2850 cm^{-1}+2930 cm^{-1}) (Fig. 4B). The band at 2850 cm^{-1} results from C–H symmetric stretching in CH_2 groups of lipids, while the band at 2930 cm^{-1} derives from C–H symmetric stretching in CH_3 groups of lipids and proteins. All statistical parameters were expressed as mean ± standard deviation (SD). Bar charts depicting the mean and standard deviation values were created using GraphPad Prism 7. Differences between control and treated groups were assessed by one-way analysis of variance (ANOVA). The calculated ratio of 2850 cm^{-1}/(2850 cm^{-1}+2930 cm^{-1}) for the TNF-α-treated cells is slightly higher than for the control cells. The greater difference can be seen when comparing the ratio for cells incubated with 3-OPG. The ratio is much higher for cells that have been pre-treated with a pro-inflammatory agent (TNF-α + 3OPG).

In addition, the ratios 1602 cm^{-1}/(1602 cm^{-1}+1450 cm^{-1}) (Figs. 4C) and 2124 cm^{-1}/(2124 cm^{-1}+1440 cm^{-1}) (Fig. 4D) were calculated. We selected the Raman band at 1440 cm^{-1}, which results from CH_2/CH_3 bending vibrations of lipids and proteins, and therefore its intensity comes from the majority of cell components presented in the cytoplasmic region. Both ratios, which indicate the 3-OPG uptake, are much higher for stimulated cells in normal conditions (3-OPG) in comparison to inflamed cells (TNF-α + 3-OPG). For cells, without glucose incubation (control and TNF-α) these ratios are 0 due to the absence of these bands. This relationship indicates a lower uptake of glucose by inflamed cells and follows that inflammation reduces the ability of EC to metabolize glucose.

Studies on live biological systems are always preferred because they represent the nearest physiological state. It is an essential step toward a better understanding of the functional processes evaluated in cells. However, due to the relatively limited lifespan of cells and variations in the biochemical and biological processes that take place inside them, researching living cells is not always practical. This is the rationale behind the widespread use of fixation techniques. To protect cellular components from e.g. bacterial decomposition and self-digestion, fixation is utilized to preserve both their structure and biological composition (Bik et al., 2020). For the measurement of living cells, additional

equipment is required to maintain stable conditions of temperature and humidity for live-cell culture.

To verify whether our proposed Rp can be used in fixed cells, in the next step the alkylated glucose has been administrated to live HAEC cells and then fixed with 2.5% glutaraldehyde (Fig. 5). Such research is particularly important as there are examples of other Rp with an affinity for mitochondria for which the changes in live versus fixed cells were observable, making it impossible, at times, to use these markers to measure fixed cells. (Li et al., 2015; Yamakoshi et al., 2015; Zeng et al., 2018). The biggest discrepancy between the spectra and the images showing the distribution of cellular components between live and fixed cells is the very weak signal from cytochrome *c*, caused by fixation due to its oxidation (Bik et al., 2020). It is also worth noting that the signal from 1602 cm^{-1} and 2124 cm^{-1} bands are also slightly weaker on Raman spectra of fixed cells, but these changes are not statistically important (Fig. 5B–C). The obtained results confirm the usefulness of the presented probe, also for tracking changes in fixed cells, in which metabolism has been 'frozen' at a full stage and this stage we can study. The occurrence of the 1602 cm^{-1} band in the spectra of fixed cells may also suggest that this band is related to the glucose metabolites. Previously, it has been indicated that Raman spectroscopic signature of life could serve as a marker of sterol metabolism but this was demonstrated in yeast cells (Chiu et al., 2012). Therefore, our hypothesis that this band is a reflection of cellular activity seems to be correct. These observations can be also supported by the fact that these cells have a relatively low content of mitochondria (6–18%) (Rajendran et al., 2013; Wong et al., 2017; Yetkin-Arik et al., 2019), which additionally lose their activity by fixation (Bik et al., 2020; Morimoto et al., 2019). The band 1602 cm^{-1} could also be a sign of pH changes inside the cells (Wen et al., 2021).

An uptake of 3-OPG by untreated and TNF-α pre-treated fixed cells was also studied employing SRS (Fig. 6). The analysis of the SRS images (Fig. 6A) enables the visualization of proteins, lipids, amino acids/proteins, 3-OPG, and its metabolic markers (1602 cm^{-1}). For better visualization and analysis of colocalization of observed compartments, the SRS images (Fig. 6A) were shown as the merged ones of proteins (2930 cm^{-1}, grey), lipids (2850 cm^{-1}, green), 3-OPG (2124 cm^{-1}, red) and *Raman spectroscopic signature of life* (1602 cm^{-1}, blue). In the case of cells incubated with 3-OPG, an intense signal from bands 2124 cm^{-1} and 1602 cm^{-1}, was observed, which is not present in the control cells and preincubated with TNF-α. More LDs were observed in cells preincubated with TNF-α as a response to stress. The intensity of 2124 cm^{-1} and 1602 cm^{-1} signals decreases for cells preincubated with TNF and then incubated with 3-OPG.

To confirm the composition of observed changes, the SRS spectra in the fingerprint region (1400-1700 cm^{-1}), silent region (2100-2200 cm^{-1}), and C–H stretching region (2800-3050 cm^{-1}) were collected (Fig. 6B). Analysis of SRS spectra of control and inflamed cells incubated with 3-OPG shows that the signal decreases, both for 2124 cm^{-1} and 1602 cm^{-1} bands. It is also worth noting that when comparing the SRS images, the co-localization of the signal from 1602 cm^{-1} and 2124 cm^{-1} bands was observed, which was not so clear in the Raman images. This may indicate that in fact, 3-OPG allows to track of the metabolites of modified glucose in endothelial cells.

Similarly, as in the case of data collected using RM, a ratiometric analysis (Fig. 6C) was performed on SRS images. To compare signatures of inflammation induced by TNF-α in HAEC and its effect on 3-OPG uptake in terms of lipid accumulation, intensity ratios of bands at 2850 cm^{-1} and 2930 cm^{-1} were determined (2850 cm^{-1}/(2850 cm^{-1} + 2930 cm^{-1}) and ratio presented in Fig. 6D). The ratio for the TNF-α-treated cells is slightly higher than that for the control cells. The greater difference can be seen when comparing the ratios for cells incubated with 3-OPG. The ratio is greater for cells that have been pre-treated with a pro-inflammatory agent.

In addition, the ratios 1602 cm^{-1}/(1602 cm^{-1} + 2930 cm^{-1}) (Figs. 6E) and 2124 cm^{-1}/(2124 cm^{-1} + 2930 cm^{-1}), (Fig. 6F), were also calculated. Both ratios calculated for bands originating from alkyne glucose (1602 and 2124 cm^{-1}) show that pre-treatment with the pro-inflammatory factor reduces the intensity of selected bands. It means that inflammation reduces the ability of ECs to uptake glucose. Importantly, it should be noted that cells of different origins or like in this case with changed functions, may have different glucose metabolism. In his work, Hu et al. (2015) emphasized that glucose uptake may be a marker of the assessment of tumor malignancy, as cancer cells with different phenotypes differ in terms of the level of glucose uptake. In HeLa and U-87 MG cells, Hu et al. showed that the latter, which belong to the group of malignant cells, give a more intense signal of 3-OPG, and thus confirmed a higher level of glucose uptake and subsequent metabolism by these cells.

Both used spectroscopic techniques enabled the acquisition of spectral information from cells, but SRS imaging increased the measurement speed, making this method optimal for this type of research.

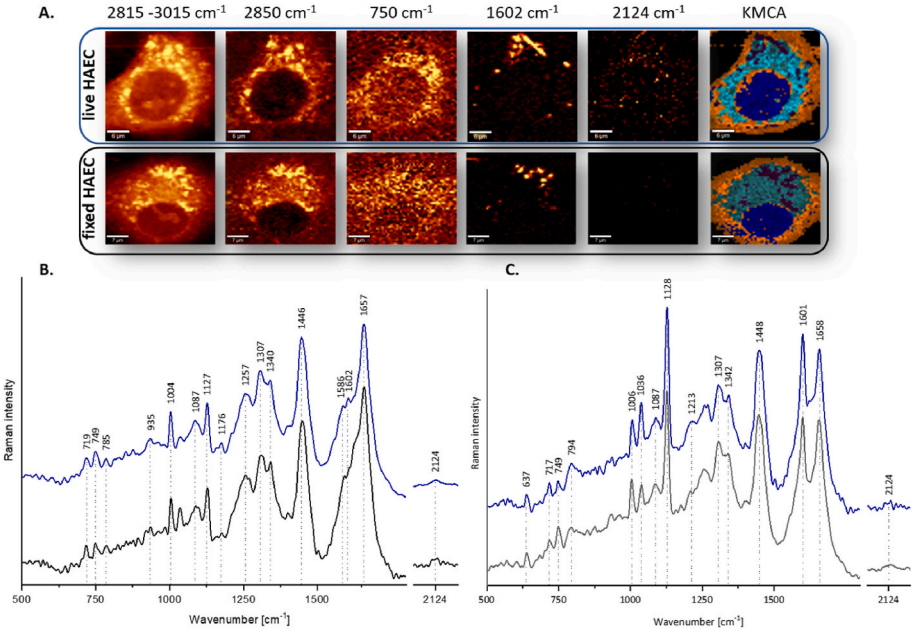

Fig. 5. A. Raman images of live and fixed HAEC cells incubated with 3-OPG (25 mM), obtained by the integration of Raman bands over the selected Raman bands at 2930 cm^{-1} (organic matter), 2850 cm^{-1} (lipids), 750 cm^{-1} (cytochrome *c*), 1602 cm^{-1} (glucose metabolite) and 2124 cm^{-1} (3-OPG), and cluster map. B. The averaged spectra of the cytoplasm region and C. Raman spectroscopic signature of glucose metabolite were defined by a 1602 cm^{-1} band of live (blue) and fixed (grey) HAEC.

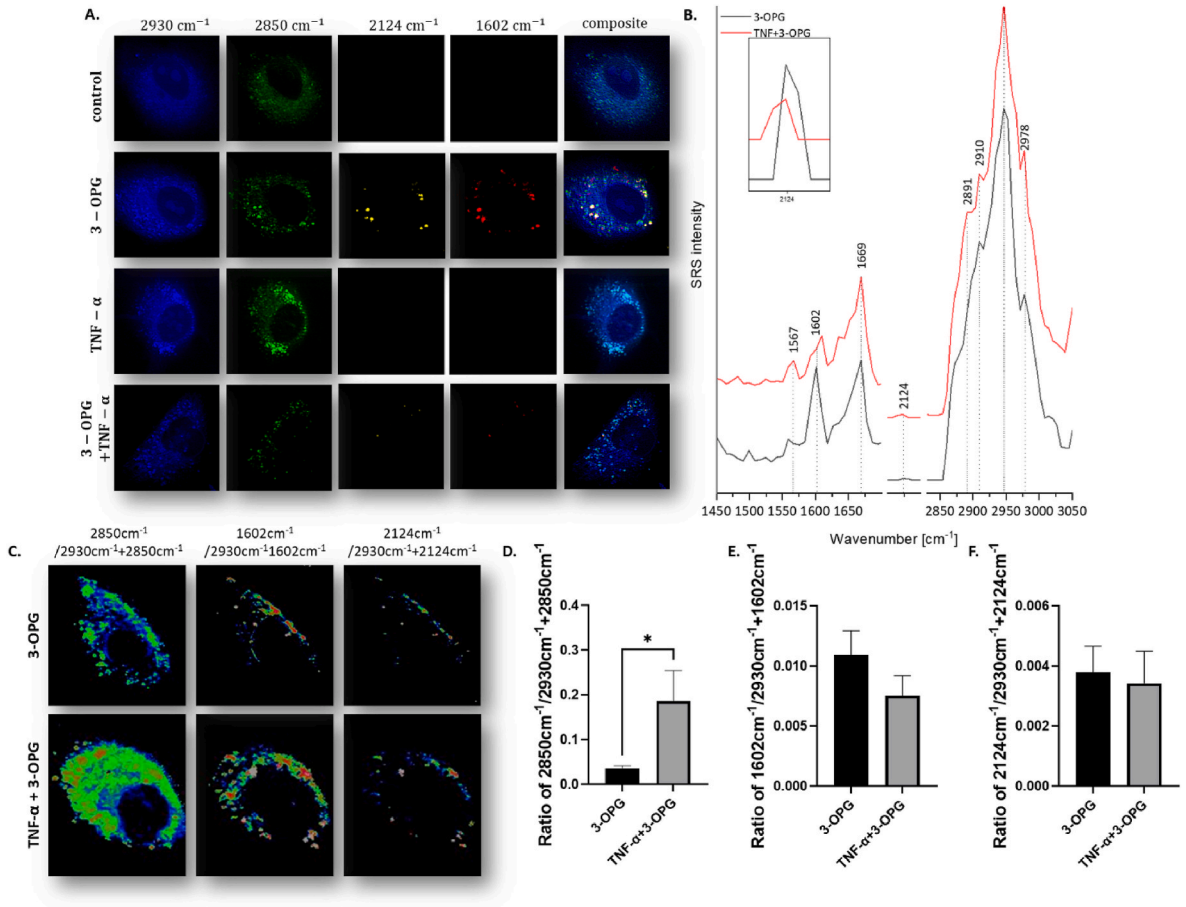

Fig. 6. A. SRS images of fixed HAEC cells for control, incubated with 3-OPG (25 mM, 24h), TNF-α (3h), and 3-OPG + TNF-α. B. Raw SRS spectra for 3-OPG (black line) and TNF-α+3-OPG (red line). C. Ratiometric SRS images representing the distribution of lipids, glucose metabolite, and alkyne group. Quantitative ratiometric analysis of the ratio of D. 2850 cm^{-1}/2930 cm^{-1}+2850 cm^{-1}, E. 1602 cm^{-1}/2930 cm^{-1}+1602 cm^{-1} and F. 2124 cm^{-1}/2930 cm^{-1}+2124 cm^{-1} for SRS images. Error bar: standard deviation. *p ≤ 0.05.

4. Conclusions

In this work, we use the alkyne-labeled glucose, 3-OPG, as a sensor to simultaneously follow its accumulation and metabolism, in both live and fixed HAECs. To the best of our knowledge, this is the first report showing the ability to track glucose metabolic changes in single ECs. We applied two experimental techniques here, i.e. spontaneous Raman imaging and SRS microscopy. Both of the spectroscopic techniques used enabled the acquisition of spectral information from cells, but SRS imaging increased the measurement speed, making this method optimal for this type of research. Previously, the 3-OPG sensor and SRS microscopy were used to distinguish cancer cells (Hu et al., 2015; Long et al., 2017). It has also been demonstrated that the mechanism of glucose uptake by various types of tissues is different (Hu et al., 2015). Here, 3-OPG was applied to ECs and, in addition to its accumulation, we were able to see its contribution to cell metabolism. Glucose uptake was followed by the characteristic Raman band of 3-OPG at 2124 cm^{-1}. It is worth emphasizing that the low intensity of the signal made it difficult to determine the exact localization of the modified glucose inside the cell, but it was found to accumulate strongly in the perinuclear region, which may be correlated to the ER. As a result of the metabolic transformation of glucose in the cell, we observed a band of 1602 cm^{-1} band, named by Hamaguchi et al. (Huang et al., 2004) as the *Raman spectroscopic signature of life*. Previously, this band was attributed to mitochondrial activity in yeast cells (Huang et al., 2007, 2004). We hypothesize that the 1602 cm^{-1} band is directly related to the presence of glucose metabolites in the cell. This was confirmed by measurements of fixed cells, for which this band is also occurring in the spectra. In our study, the 1602 cm^{-1} band is strong, so it can undoubtedly be detected in the complex cellular spectrum. Additionally, we have shown that by inducing stress in cells, e.g. as a result of inflammation, there is a slowdown in cellular metabolism (as evidenced by the lowering of the intensity of the bands at 1602 and 2124 cm^{-1}). Taken together, our results prove that 3-OPG can be considered as a Raman sensor to study glucose metabolism in cells in a sensitive and specific way.

CRediT authorship contribution statement

Anna Pieczara: Measurements, Formal analysis, Investigation, Visualization, Writing – original draft. **Aleksandra Borek-Dorosz:** Formal analysis, Investigation, Writing – original draft. **Szymon Buda:** 3-OPG synthesis, Writing – review & editing. **William Tipping:** Data curation, Writing – review & editing. **Duncan Graham:** Writing – review & editing. **Robert Pawlowski:** Writing – review & editing. **Jacek Mlynarski:** Supervision, over 3-OPG synthesis, Writing – review & editing. **Malgorzata Baranska:** Financing, Supervision, Conceptualization, Investigation, Writing – review & editing.

Declaration of competing interest

The authors declare that they have no known competing financial interests or personal relationships that could have appeared to influence the work reported in this paper.

Data availability

Data will be made available on request.

Acknowledgment

This work was supported by a grant from the National Science Center Poland (NCN) (OPUS15 no. UMO-2018/29/B/ST4/00335 to Malgorzata Baranska) and by the Visibility&Mobility module under the program "Excellence Initiative – Research University" at the Jagiellonian University in Krakow.

The open-access publication of this article has been supported by a grant from the Faculty of Chemistry under the Strategic Programme Excellence Initiative at Jagiellonian University.

The authors are grateful to MSc Renata Budzynska (JCET UJ) for cell culture maintenance and Adrianna Wislocka-Orlowska for technical support.

Appendix A. Supplementary data

Supplementary data to this article can be found online at https://doi.org/10.1016/j.bios.2023.115234.

References

Ao, J., Feng, Y., Wu, S., Wang, T., Ling, J., Zhang, L., Ji, M., 2020. Small Methods 4, 1900600.
Awual, M.R., 2019a. J. Environ. Chem. Eng. 7, 103124.
Awual, M.R., 2019b. Mater. Sci. Eng. C 101, 686–695.
Awual, M.R., 2017. Chem. Eng. J. 307, 85–94.
Baranska, M., Kaczor, A., Malek, K., Jaworska, A., Majzner, K., Staniszewska-Slezak, E., Pacia, M.Z., Zajac, G., Dybas, J., Wiercigroch, E., 2015. Pharmacol. Rep. 67, 736–743.
Bik, E., Dorosz, A., Mateuszuk, L., Baranska, M., Majzner, K., 2020. Spectrochim. Acta Part A Mol. Biomol. Spectrosc. 240, 118460.
Bik, E., Orleanska, J., Mateuszuk, L., Baranska, M., Majzner, K., Chlopicki, S., 2022. Biochim. Biophys. Acta Mol. Cell Res. 1869, 119186.
Bleesing, J.J.H., Fleisher, T.A., 2001. Semin. Hematol. 38, 100–110.
Borek-Dorosz, A., Pieczara, A., Czamara, K., Stojak, M., Matuszyk, E., Majzner, K., Brzozowski, K., Bresci, A., Polli, D., Baranska, M., 2022. Cell. Mol. Life Sci. 79, 593.
Brzozowski, K., Matuszyk, E., Pieczara, A., Firlej, J., Nowakowska, A.M., Baranska, M., 2022. Biotechnol. Adv. 60, 108003.
Chiu, L. da, Ando, M., Hamaguchi, H.o., 2010. J. Raman Spectrosc. 41, 2–3.
Chiu, L. Da, Hamaguchi, H.O., 2011. J. Biophot. 4, 30–33.
Chiu, L. da, Hullin-Matsuda, F., Kobayashi, T., Torii, H., Hamaguchi, H.o., 2012. J. Biophot. 5, 724–728.
Czamara, K., Majzner, K., Selmi, A., Baranska, M., Ozaki, Y., Kaczor, A., 2017. Sci. Rep. 71 7, 1–10, 2017.
Du, W., Ren, L., Hamblin, M.H., Fan, Y., 2021. Biomedicines 9, 147.
Eelen, G., De Zeeuw, P., Simons, M., Carmeliet, P., 2015. Circ. Res. 116, 1231–1244.
Fleury, G., Roeffaers, M.B.J., 2020. Catalysts 10, 1–12.
Freudiger, C.W., Min, W., Saar, B.G., Lu, S., Holtom, G.R., He, C., Tsai, J.C., Kang, J.X., Xie, X.S., 2008. Science 322, 1857–1861.
Galley, H.F., Webster, N.R., 2004. Br. J. Anaesth. 93, 105–113.
Grammel, M., Hang, H.C., 2013. Chemical reporters for biological discovery. Nat. Chem. Biol. 9, 475–484.
Hamada, K., Fujita, K., Smith, N.I., Kobayashi, M., Inouye, Y., Kawata, S., 2008. J. Biomed. Opt. 13, 044027.
Hamaguchi, H.o., Iwata, K., 2017. Encycl. Spectrosc. Spectrom. 463–468.
Hasan, M.M., Shenashen, M.A., Hasan, M.N., Znad, H., Salman, M.S., Awual, M.R., 2021. J. Mol. Liq. 323, 114587.
Hu, F., Chen, Z., Zhang, L., Shen, Y., Wei, L., Min, W., 2015. Angew. Chem. Int. Ed. 54, 9821–9825.
Hu, F., Lamprecht, M.R., Wei, L., Morrison, B., Min, W., 2016. Sci. Rep. 6, 39660.
Huang, Y.S., Karashima, T., Yamamoto, M., Hamaguchi, H.O., 2003. J. Raman Spectrosc. 34, 1–3.
Huang, Y.S., Karashima, T., Yamamoto, M., Ogura, T., Hamaguchi, H.O., 2004. J. Raman Spectrosc. 35, 525–526.
Huang, Y.S., Nakatsuka, T., Hamaguchi, H.O., 2007. Appl. Spectrosc. 61, 1290–1294.
Jamieson, L.E., Greaves, J., McLellan, J.A., Munro, K.R., Tomkinson, N.C.O., Chamberlain, L.H., Faulds, K., Graham, D., 2018a. Spectrochim. Acta Part A Mol. Biomol. Spectrosc. 197, 30–36.
Jamieson, L.E., Wetherill, C., Faulds, K., Graham, D., 2018b. Chem. Sci. 9, 6935–6943.
Ji, M., Orringer, D.A., Freudiger, C.W., Ramkissoon, S., Liu, X., Lau, D., Golby, A.J., Norton, I., Hayashi, M., Agar, N.Y.R., Young, G.S., Spino, C., Santagata, S., Camelo-Piragua, S., Ligon, K.L., Sagher, O., Sunney Xie, X., 2013. Sci. Transl. Med. 5, 201ra119.
Ji, R.C., Kato, S., 2001. Microsc. Res. Tech. 55, 70–80.
Kubra, K.T., Salman, M.S., Znad, H., Hasan, M.N., 2021. J. Mol. Liq. 329, 115541.
Lalonde, J.W., Noojin, G.D., Pope, N.J., Powell, S.M., Yakovlev, V.V., Denton, M.L., 2021. J. Biophot. 14, e202000384.
Laptenok, S.P., Martin, C., Genchi, L., Duarte, C.M., Liberale, C., 2020. Environ. Pollut. 267, 115640.
Li, Y., Heo, J., Lim, C.K., Pliss, A., Kachynski, A.V., Kuzmin, A.N., Kim, S., Prasad, P.N., 2015. Biomaterials 53, 25–31.
Li, Y., Wang, Z., Mu, X., Ma, A., Guo, S., 2017. Raman tags: novel optical probes for intracellular sensing and imaging. Biotechnol. Adv. 35, 168–177.
Liao, C.S., Cheng, J.X., 2016. Annu. Rev. Anal. Chem. 9, 69–93.
Long, R., Zhang, L., Shi, L., Shen, Y., Hu, F., Zeng, C., Min, W., 2017. Chem. Commun. 54, 152–155.
Małek, K., 2016. Vibrational Spectroscopy: from Theory to Applications. Wydawnictwo Naukowe PWN.
Matuszyk, E., Adamczyk, A., Radwan, B., Pieczara, A., Szcześniak, P., Mlynarski, J., Kamińska, K., Baranska, M., 2021. Spectrochim. Acta Part A Mol. Biomol. Spectrosc. 255, 119658.
Miao, Y., Qian, N., Shi, L., Hu, F., Min, W., 2021. Nat. Commun. 12, 4518.
Morimoto, T., Chiu, L., Da, Kanda, H., Kawagoe, H., Ozawa, T., Nakamura, M., Nishida, K., Fujita, K., Fujikado, T., 2019. Analyst 144, 2531–2540.
Pacia, M.Z., Sternak, M., Mateuszuk, L., Stojak, M., Kaczor, A., Chlopicki, S., 2020. Biochim. Biophys. Acta Mol. Cell Res. 1867, 118681.
Palonpon, A.F., Sodeoka, M., Fujita, K., 2013. Molecular imaging of live cells by Raman microscopy. Curr. Opin. Chem. Biol. 17, 708–715.
Pircher, A., Treps, L., Bodrug, N., Carmeliet, P., 2016. Atherosclerosis 253, 247–257.
Pober, J.S., Sessa, W.C., 2007. Nat. Rev. Immunol. 7, 803–815.
Potente, M., Carmeliet, P., 2017. Annu. Rev. Physiol. 79, 43–63.
Prescher, J.A., Bertozzi, C.R., 2005. Nat. Chem. Biol. 1, 13–21.
Pully, V.V., Otto, C., 2009. J. Raman Spectrosc. 40, 473–475.
Rajendran, P., Rengarajan, T., Thangavel, J., Nishigaki, Y., Sakthisekaran, D., Sethi, G., Nishigaki, I., 2013. Int. J. Biol. Sci. 9 (10), 1057–1069.
Raman, C.V., Krishnan, K.S., 1928. A new type of secondary radiation. Nature 121, 501–502.
Sato, H., Ishigaki, M., Taketani, A., Andriana, B.B., 2019. Biomed. Spectrosc. Imag. 7, 97–104.
Seydel, C., 2021. Nat. Methods 18, 1452–1456.
Theodoridis, G., Gika, H.G., Wilson, I.D., 2011. Mass Spectrom. Rev. 30, 884–906.
Wang, C., Liu, H., Yang, M., Bai, Y., Ren, H., Zou, Y., Yao, Z., Zhang, B., Li, Y., 2020. Eur. J. Vasc. Endovasc. Surg. 59, 834–842.
Wang, Ping, Li, J., Wang, Pu, Hu, C.-R., Zhang, D., Sturek, M., Cheng, J.-X., 2013. Angew. Chem. 125, 13280–13284.
Wei, L., Chen, Z., Shi, L., Long, R., Anzalone, A.V., Zhang, L., Hu, F., Yuste, R., Cornish, V.W., Min, W., 2017. Nature 544, 465–470.
Wei, L., Hu, F., Chen, Z., Shen, Y., Zhang, L., Min, W., 2016. Acc. Chem. Res. 49, 1494–1502.
Wei, L., Hu, F., Shen, Y., Chen, Z., Yu, Y., Lin, C.C., Wang, M.C., Min, W., 2014. Nat. Methods 11, 410–412.
Wen, C., Yu, C., Thirumalaivasan, N., Hiramatsu, H., 2021. J. Raman Spectrosc. 52, 641–654.
Wong, B.W., Marsch, E., Treps, L., Baes, M., Carmeliet, P., 2017. EMBO J. 36, 2187–2203.
Yamakoshi, H., Dodo, K., Palonpon, A., Ando, J., Fujita, K., Kawata, S., Sodeoka, M., 2012. J. Am. Chem. Soc. 134, 20681–20689.
Yamakoshi, H., Palonpon, A., Dodo, K., Ando, J., Kawata, S., Fujita, K., Sodeoka, M., 2015. Bioorg. Med. Chem. Lett 25, 664–667.
Yetkin-Arik, B., Vogels, I.M.C., Nowak-Sliwinska, P., Weiss, A., Houtkooper, R.H., Van Noorden, C.J.F., Klaassen, I., Schlingemann, R.O., 2019. Sci. Rep. 9, 1–14.
Zeng, C., Hu, F., Long, R., Min, W., 2018. Analyst 143, 4844–4848.
Zhang, L., Shi, L., Shen, Y., Miao, Y., Wei, M., Qian, N., Liu, Y., Min, W., 2019. Nat. Biomed. Eng. 3, 402–413.
Zhang, X., Roeffaers, M.B.J., Basu, S., Daniele, J.R., Fu, D., Freudiger, C.W., Holtom, G. R., Xie, X.S., 2012. ChemPhysChem 13, 1054–1059.
Zhu, G., Zhu, X., Fan, Q., Wan, X., 2011. Spectrochim. Acta Part A Mol. Biomol. Spectrosc. 78, 1187–1195.
Zhu, J., Thompson, C.B., 2019. Nat. Rev. Mol. Cell Biol. 20, 436–450.